

Original article

Investigation of coal elastic properties based on digital core technology and finite element method

Ahmada Bacar Andhumoudine¹, Xin Nie^{1,2}, Qingbo Zhou³, Jie Yu^{1,4}, Oumar Ibrahima Kane¹, Longde Jin⁵, Roufida Rana Djaroun¹

¹Key Laboratory of Exploration Technologies for Oil and Gas Resources (Yangtze University), Wuhan 430100, P. R. China

²Cooperative Innovation Center of Unconventional Oil and Gas, Yangtze University, Wuhan 430100, P. R. China

³China France Bohai Geoservices Co., Ltd, Tianjin 300457, P. R. China

⁴CNOOC Research Institute, Beijing 100027, P. R. China

⁵Golder Associates, Atlanta, Georgia 30341, USA

Keywords:

Coalbed
elastic property
digital core
micro-CT
finite element method
numerical simulation

Cited as:

Andhumoudine, A. B., Nie, X., Zhou, Q., Yu, J., Kane, O. I., Jin, L., Djaroun, R. R. Investigation of coal elastic properties based on digital core technology and finite element method. *Advances in Geo-Energy Research*, 2021, 5(1): 53-63, doi: 10.46690/ager.2021.01.06

Abstract:

Rock elastic properties play an important role in the geological characteristics of reservoirs. The analysis of these properties is normally based physical experiments on rocks. However, such conventional physical experiments cannot meet actual requirements when the rock is fragile or has complex composition. With the development of computer technology and the application of micro-computed tomography scanning technology, digital rock physics technologies came into existence. In this work, micro-computed tomography was applied to obtain high-quality three-dimensional images of coal samples. Next, the image multi-threshold segmentation method was used to divide the grayscale image into three reasonable components, including mineral, organic matrix, and pores. Digital rock models with different gas saturations were established using mathematical morphology based methods. Five volume samples were selected from the original large digital rock model under different conditions of porosity, mineral, and gas saturation. Based on these three-dimensional digital cores and the finite element method, the effective elastic moduli of coal rock mass were simulated and the compressional wave velocity and shear wave velocity were computed. Results show that, in the absence of filled minerals, both bulk and shear moduli decrease with rising porosity; compressional and shear wave velocities decline, and the ratio of compressional wave velocity to shear wave velocity increases. However, a more realistic study considering filled minerals demonstrates decreasing shear wave velocity and counterintuitively rising compressional wave velocity when the porosity increases. Gas saturation only affects the compressional wave velocity. The obtained results improve our understanding of rock elastic behaviors in the coalbed.

1. Introduction

The coalbed and its by-products are processed and used in several industries to generate electricity, or to produce fertilizers and plastics. Coal can also be transformed into diesel and gasoline fuel used for motorized vehicles in many countries in the world, including Canada, USA, Australia, India, and China (Gentzis and Bolen, 2008; Moore, 2012; Peng et al., 2017; Cui et al., 2018; Vishal et al., 2018).

The elastic properties of reservoir rocks are important for

seismic interpretation, reservoir evaluation and reserve estimation (Wang et al., 2013b; Wang and Fehler, 2018). According to Al-Marzouqi (2018), the very small-scale structure of a rock is a paramount aspect controlling its physical behavior. Valuable insights can be gained into the comprehension and evaluation of rock physical properties by the understanding of pore-scale physics. Routine experiments can be carried out to regulate the elastic parameters of a coal reservoir. However, some complications remain that have a certain impact on such experiments: the loose structure of coal rock is not favorable

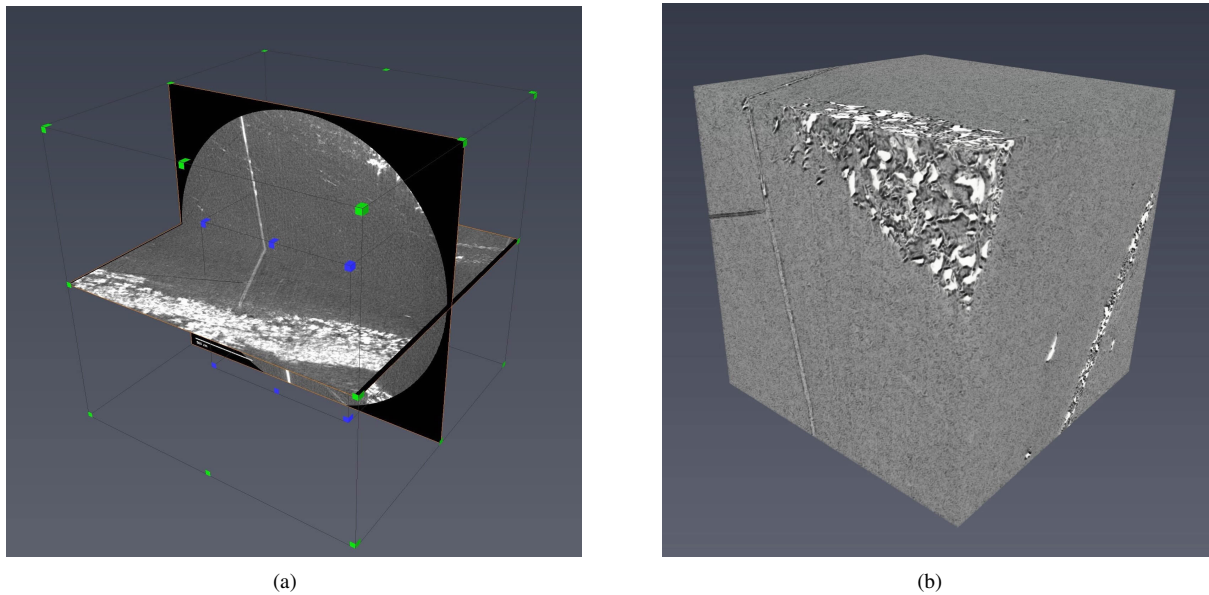


Fig. 1. Extraction location of model rendering (a) and cropped unit (b).

for collection and sample preparation; when ultrasonic testing processes are applied to the rock, the coal structure can be destroyed, and its energy state will considerably weaken, thus making the extraction of affective waveform data beyond the bounds of possibility (Chauhan et al., 2016). Numerous physical properties can be assessed based on digital rock physics (DRP), which supply high resolution computed tomography (CT) images of the rock pore and mineral geometries (Al-Marzouqi, 2018; Dvorkin, 2020). Techniques of DRP have been used to enhance the petrophysical properties of rocks and porous media in different materials (Chen and Zhou, 2017; Sun et al., 2017). Based on digital core models, the effective electrical conductivity or elasticity can be simulated with the finite element method (FEM) (Wang et al., 2013a; Nie et al., 2016, 2019; Wei et al., 2018). Researchers have used DRP to study the elastic properties of simple rocks such as sandstones (Arns, 2002; Makarynska et al., 2008; Combaret et al., 2013; Madonna et al., 2013; Zhao et al., 2020). Recently, digital core technology has also been applied by many researchers on anisotropy rocks, such as fractured rocks, thinly bedded rocks, and shale gas reservoir (Zhao et al., 2013; Sun et al., 2014; Nie et al., 2016; Zhang et al., 2016; Wei et al., 2018). Nonetheless, few studies have focused on coal elastic property simulations.

In this study, the elastic properties of coalbed methane reservoir rocks are obtained based on three-dimensional (3D) digital cores. First, 3D digital core models of coals are built by micro-CT scanning, and the gray-scale voxels are segmented into pore, organic matrix, and mineral. Next, the pore is separated into gas and water with the mathematical morphological method (Section 2). Different elastic moduli are assigned to different respective components, and the equivalent elastic moduli of the models are calculated using the FEM (Section 3). Finally, effects of different component contents are also explored and discussed (Section 3).

2. Methodology

2.1 Micro-CT scan

Micro-CT scanning is used to reconstruct computer images, so that the information of materials with different densities on the specified level are displayed in the form of high-resolution digital images. In this study, the coal rock sample was obtained from Qinshui Basin, China. The rock sample was 1.88 mm in diameter, and the CT scanning 3D image had a resolution of 1.95 μm . Once the core sample image was acquired, a $500 \times 500 \times 500$ voxel-sized cuboid was cropped out for better imaging. The extraction location of the cropped unit can be seen on the left side, whereas the image of the cropped unit is the right side of Fig. 1.

2.2 Image processing

Various types of system noise are present in the grayscale image of the core obtained by micro-CT scanning, which reduce image quality and are not conducive to subsequent quantitative analysis (Maximenko and Kadet, 2000). Therefore, CT images were processed using three filtering algorithms: median filtering, low-pass linear filtering, and Gaussian smoothing filtering. The filtering effects of the above three algorithms were comprehensively compared to select different filtering algorithms in combination with different types of images to be processed (Huang et al., 1979). After filtering, the grayscale image is conducive to the natural transition between pore and skeleton, and it can also make the boundary smooth and retain the characteristic information of the image. In order to better quantify and distinguish the skeleton and the pores, however, it is necessary to further use the image segmentation method to perform a reasonable labeling processing of the gray image. The key to image labeling is to select the segmentation thresholds from coal porosity and mineral content based on experimental laboratory data. The final thresholds data should

make the segmentation result close enough to experimental core porosity and component data. Taking the final searched value as the multi-segmentation thresholds, the segmented labeled image is obtained, including pore, mineral, and organic matrix. The image after threshold segmentation is presented in Fig. 2, where dark blue represents minerals; light blue indicates organic matrix; and red represents pores.

2.3 Simulation of fluid distribution

In the present work, the fluid distribution was simulated by a mathematical morphological method, which includes four basic operations: dilation operation, erosion operation, opening operation and closing operation, as shown in Fig. 3 (Serra, 1982; Hu et al., 2001; Liu et al., 2009). Furthermore, advanced complex algorithms based on dilation and erosion operations are useful to implement many kinds of image processing (Haralick et al., 1987; Zhang, 2017), including image classification and recognition (Icke et al., 2005), origi-

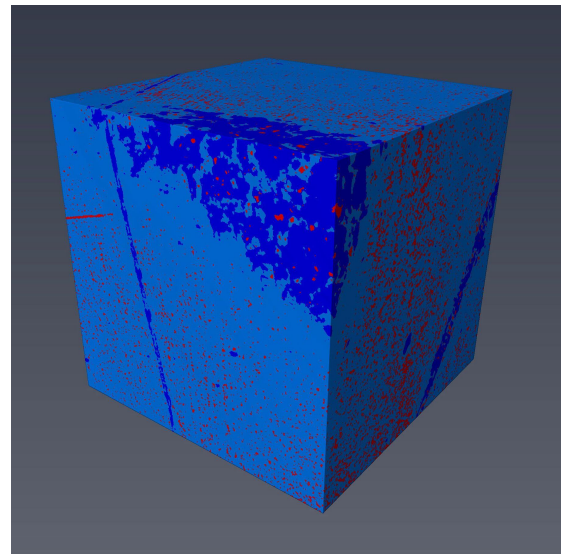
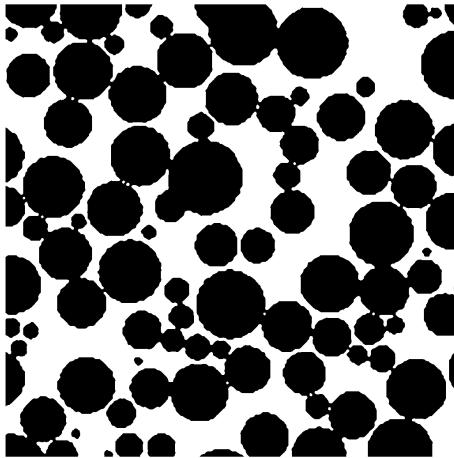
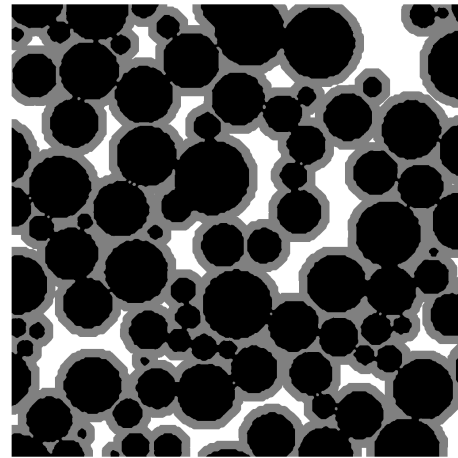


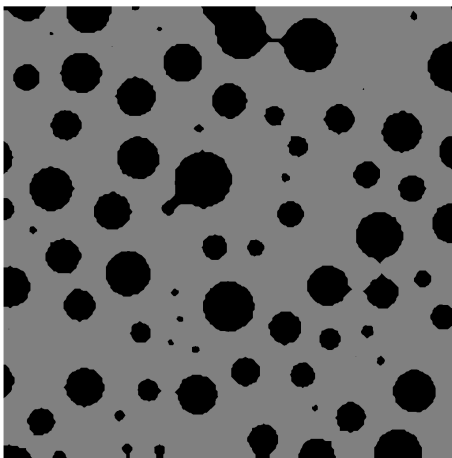
Fig. 2. Image after multi-threshold segmentation.



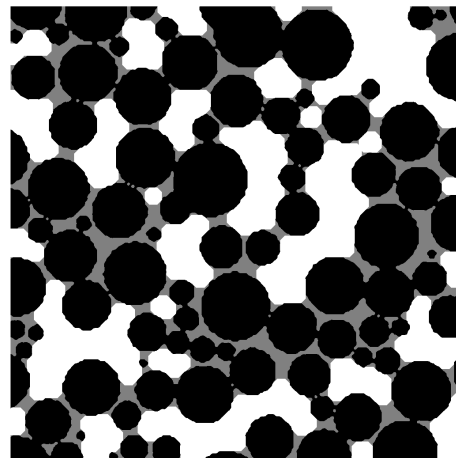
(a) Original image



(b) Erosion algorithm



(c) Dilation algorithm



(d) Opening algorithm

Fig. 3. Sketch of erosion, dilation, and opening algorithms (modified from Liu et al., 2009).

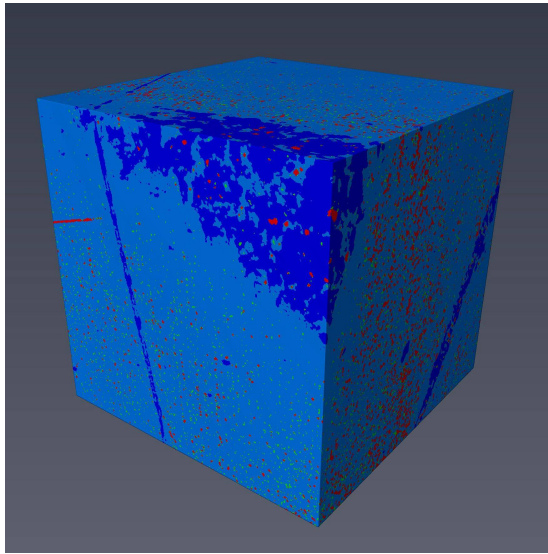


Fig. 4. Image after one opening operation.

nal image reconstruction, feature extraction, and edge detection (Wei and Tong, 2010). When constructing a three-dimensional digital core, it is usually regarded as a 2-phase model consisting only of skeleton and pore space. Mathe-

matical morphology can be used to facilitate the simulation of the pore fluid distribution of a rock (Liu et al., 2009). The mathematical morphology methods of this paper are used to simulate different saturation conditions. After a series of opening operations, the models of different gas saturations are obtained, as seen in Fig. 4, where green indicates the presence of gas and red denotes the presence of water.

Table 1. Model material parameters.

Model No.	1	2	3	4	5
Porosity	0.0496	0.1089	0.0694	0.0279	0.0213
Organic matter	0.9234	0.8280	0.8805	0.9712	0.9399
Mineral content	0.0270	0.0631	0.0501	0.0009	0.0388

2.4 Selection of sub-cores

Following the fluid distribution simulation, 5 sub-cores were selected from the original whole-core model. Table 1 details the different component volume contents of the 5 models, while Fig. 5 shows the images of the equivalent sub-cores; next-step simulations were implemented based on these models.

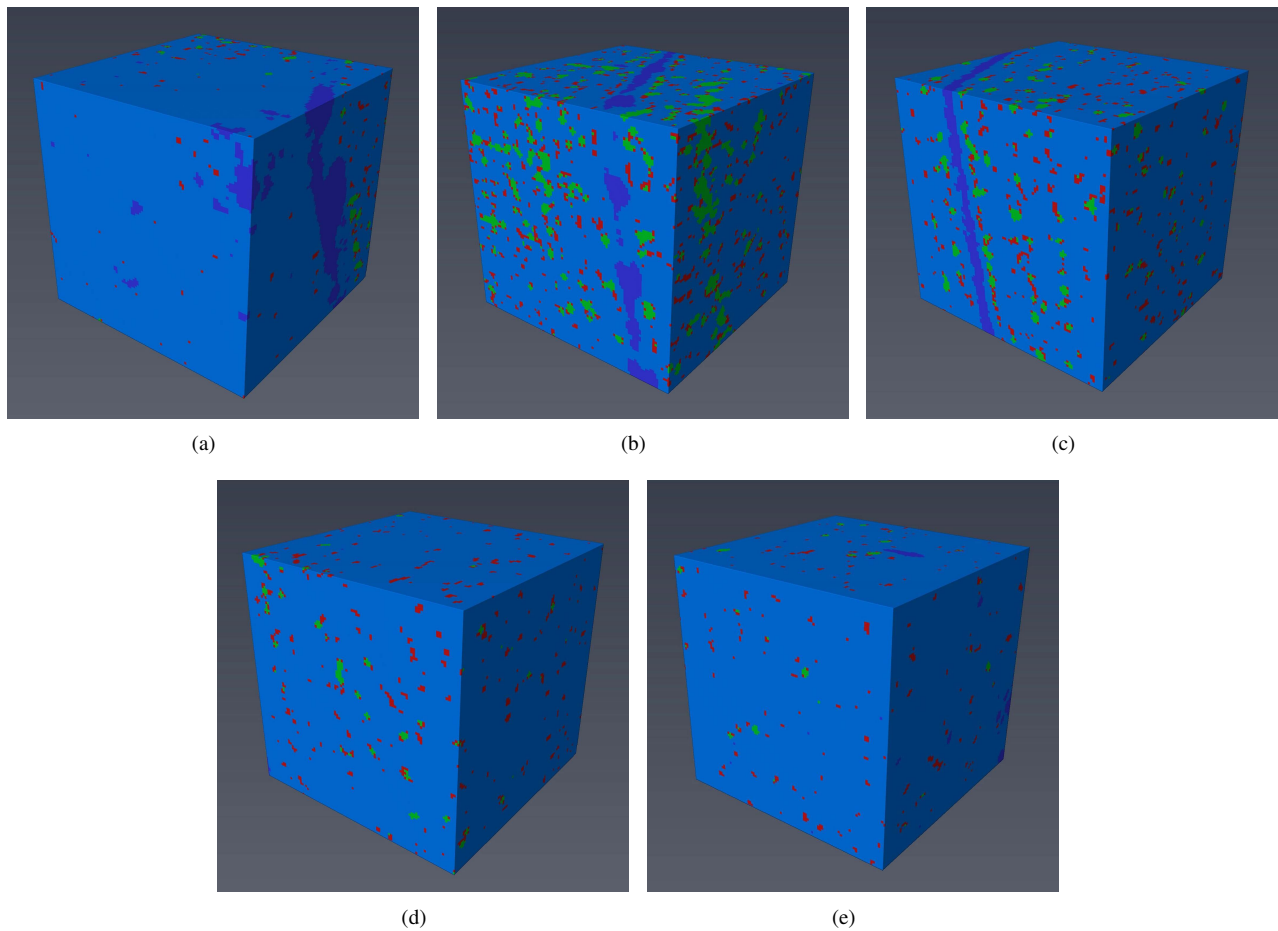


Fig. 5. Composition distribution of the 5 sub-cores.

2.5 FEM and elasticity simulation

The FEM is used to calculate the information required to obtain the effective linear random material properties and simulate the elasticity of the 3D digital core. The method was proposed by Garboczi and Day (1995) and the code is written in Fortran language. In order to calculate the finite element problem, the model needs to be divided into non-overlapping finite element units. In the digital rock cases, each voxel is set as an elemental unit, and a periodic boundary condition is adopted. Furthermore, macro-strains are applied in the principal stress direction and the shear stress direction. By using the finite element method to calculate the elastic modulus of the three-dimensional digital core, the elastic potential energy can be expressed as the quadratic polynomial of the elastic displacement vector of each node (Liu et al., 2009). The finite element method can be used to calculate stress and strain in six directions. In this paper, we use isotropic models to analyze the elastic properties. For the isotropic cases, the bulk modulus (K) and shear modulus (μ) can be obtained by the following equations:

$$K = \frac{\sigma_{xx} + \sigma_{yy} + \sigma_{zz}}{3(\varepsilon_{xx} + \varepsilon_{yy} + \varepsilon_{zz})} \quad (1)$$

$$\mu = \frac{\tau_{xy}}{\varepsilon_{xy}} \quad (2)$$

where σ_{xx} , σ_{yy} , σ_{zz} , τ_{xz} , σ_{yz} , σ_{xy} represent the stresses in 6 directions; ε_{xx} , ε_{yy} , ε_{zz} , ε_{xz} , ε_{yz} , ε_{xy} represent the strains in 6 directions.

Using the bulk modulus and the shear modulus obtained by calculation, the P wave velocity V_p and S wave velocity V_s of the three-dimensional digital core can be calculated by Eqs. (3) and (4). The average density in the formula can be multiplied by the density of the corresponding component to obtain the respective volume fraction.

$$V_p = \sqrt{\frac{K + 4/3\mu}{\rho}} \quad (3)$$

$$V_s = \sqrt{\frac{\mu}{\rho}} \quad (4)$$

3. Application results and discussion

3.1 Reliability of simulation results

In this numerical simulation experiment, based on the 3-D digital core, the equivalent elastic moduli of the rock samples

Table 2. The elastic parameters of each component.

	Porosity (gas)	Porosity (water)	Mineral (calcite)	Organic
Bulk modulus (GPa)	0.20	2.20	81.00	2.90
Shear modulus (GPa)	0.00	0.00	30.70	2.70
Density (g/cm ³)	0.30	1.00	2.71	1.30

are calculated by the finite element method; the P and S wave velocities are subsequently obtained. The moduli of methane gas, water, organic matter and mineral used in the simulations are listed in Table 2.

The final result for P and S wave velocities under dry sample condition are shown in Table 3. When evaluating the ultrasonic velocity test results of samples from the same coal rock, it can be concluded that the P and S wave velocities calculated using the numerical simulation results are within the measured values of dry samples of this coal rock. The experimental results of the core wave velocities under gas saturation are: 2190.0-3170.0 m/s (V_p) and 1040.0-1560.0 m/s (V_s). These values demonstrate that the simulation of this time value is in good agreement with the actual results.

3.2 Elastic properties under ideal conditions without mineral

In this section, the effect of porosity and gas saturation is discussed without considering the mineral by setting the same parameters for the mineral label as the organic matrix.

3.2.1 Effect of porosity

Porosity is one of the most important physical properties of coal-rock reservoir, as well as one of the most essential indicators in coal-rock reservoir evaluation. Understanding the relationship between porosity and rock elastic mechanical parameters of coal reservoirs is of great significance to actual production. Figs. 6(a)-6(b) present the results of bulk and shear moduli changing with porosity. When the porosity increases, the volume fraction of the matrix will inevitably decline. Since the bulk and shear moduli of water and gas are both lower than those of the matrix, the bulk and shear moduli show a reduction.

The relationships among V_p , V_s , and porosity are shown in Figs. 6(c)-6(d). When the porosity rises, the P and S wave

Table 3. Simulation results of the 5 gas-saturated sub-core models.

Model Number	Density (g/cm ³)	Matrix Density (g/cm ³)	Bulk modulus (GPa)	Shear modulus (GPa)	V_p (km/s)	V_s (km/s)	V_p/V_s
1	1.3109	1.3400	3.2453	2.5039	2.2410	1.3786	1.6255
2	1.3192	1.3999	3.5957	2.1996	2.2246	1.2733	1.7471
3	1.3317	1.3758	3.7110	2.4336	2.2855	1.3513	1.6913
4	1.2897	1.3013	2.8596	2.5559	2.2045	1.4022	1.5721
5	1.3461	1.3558	3.1200	2.6694	2.2275	1.4324	1.5551

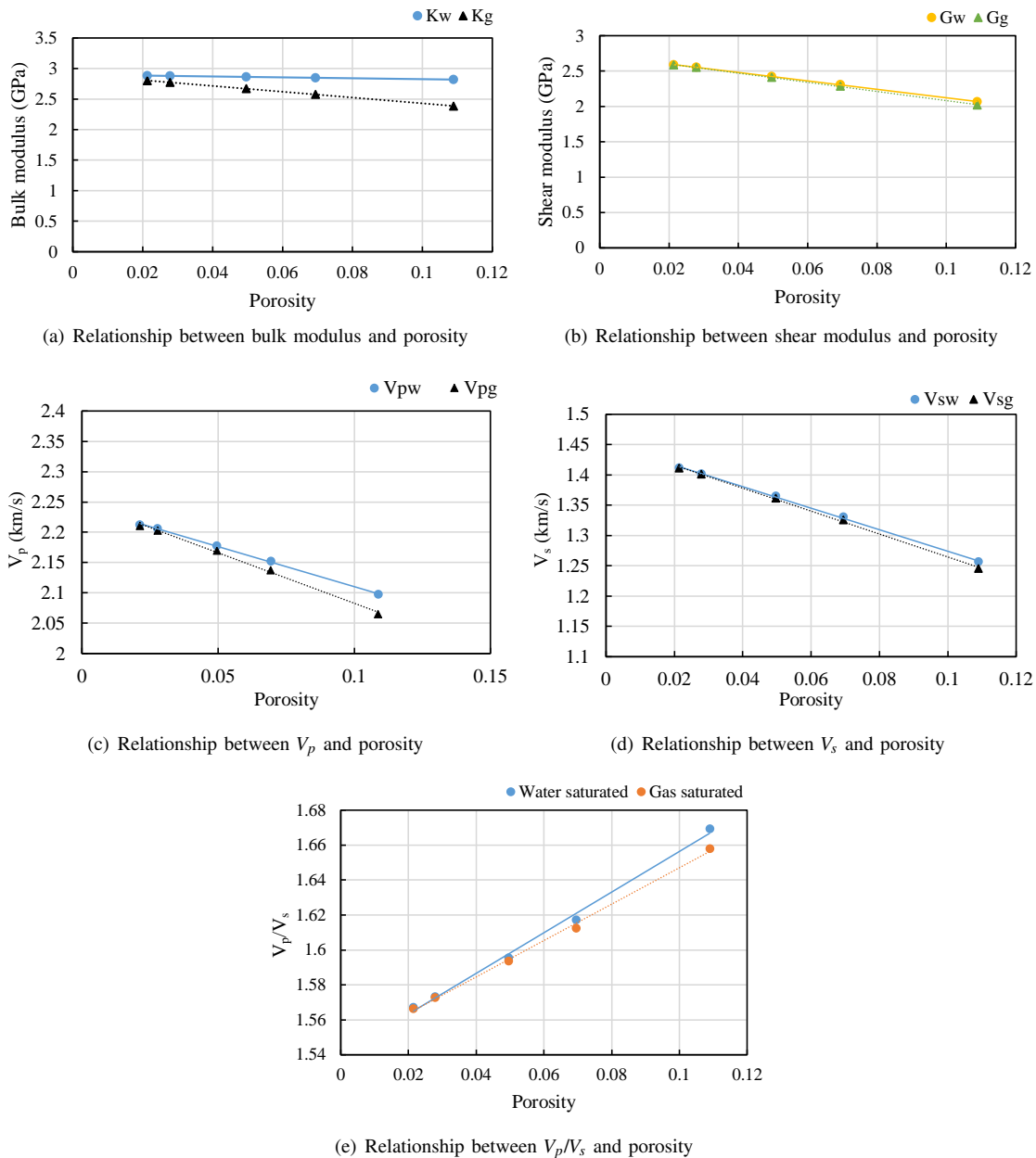


Fig. 6. Effect of porosity on elastic properties under ideal conditions.

velocities of coal rock reservoirs gradually subside, and the wave velocities under water saturation are greater than those under gas saturation. The difference between V_s under gas and water saturation is small. It can be concluded that the fluid type has a lower effect on V_s as compared to V_p . The V_p/V_s ratio increases, i.e., V_s drops faster than V_p with porosity, as shown in Fig. 6(e).

3.2.2 Effect of gas saturation

The results for bulk modulus with increasing gas saturation are shown in Figs. 7(a)-7(b); the bulk modulus decreases when the gas saturation increases, and the shear modulus remains unchanged. This is because gas and water have different bulk moduli and equal shear moduli. Therefore, gas saturation affects the bulk modulus, but barely influences the shear

modulus.

The effect of gas saturation on V_p and V_s are shown in Figs. 7(c)-7(d). Results in the figures reveal that as gas saturation increases, V_p drops while V_s remains unchanged. Therefore, the V_p/V_s ratio slightly decreases with gas saturation, as shown in Fig. 7(e).

3.3 Elastic properties under real conditions with mineral

The elastic properties under ideal conditions have been discussed without considering the minerals, even though the development of minerals in coalbeds can be a major factor affecting elastic properties. In this section, the effect of porosity and gas saturation is considered while accounting for the

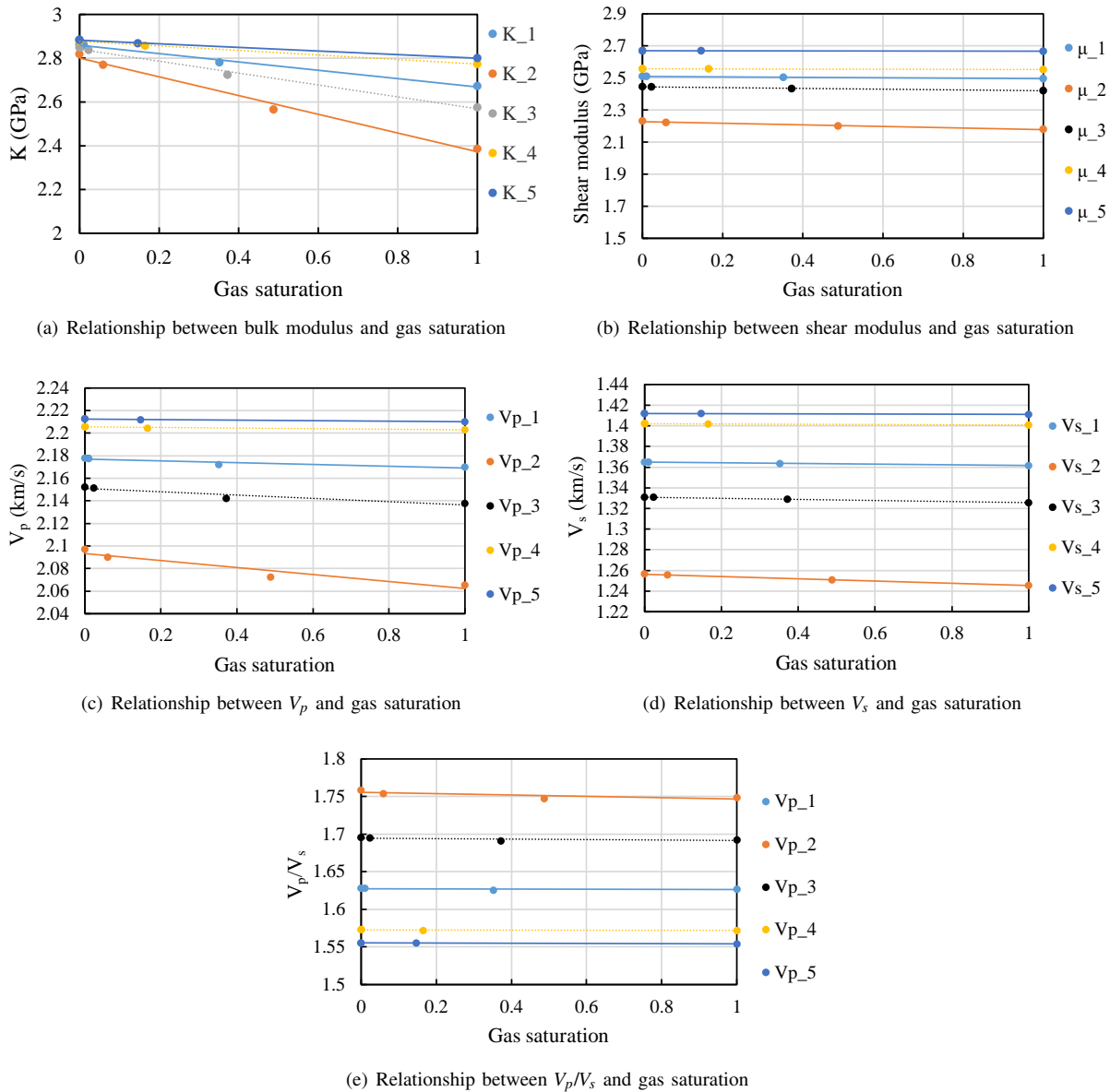


Fig. 7. Effect of gas saturation on elastic properties under ideal conditions.

presence of the minerals.

3.3.1 Effect of porosity

The relationships among bulk modulus, shear modulus and porosity are shown in Figs. 8(a)-8(b). As presented in Figs. 8(a)-8(b), when the porosity increases, the bulk modulus gradually rises and the shear modulus decreases. Under ideal conditions, the trend of bulk modulus is not consistent with these changes. It is clear from Fig. 9 that model porosity is positively related to mineral content, i.e., when porosity is higher, more mineral can develop in the microfractures or large pores. The relatively high bulk modulus of the mineral increases the effective bulk modulus. However, with declining porosity, the shear modulus still drops. In conclusion, the bulk modulus is more strongly affected by the mineral content than the shear modulus.

The effect of porosity on V_p and V_s are shown in Figs. 8(d)-8(e). When comparing these results to data on Fig. 6, it is clear that when minerals are considered, V_p and V_s will be relatively higher. Increased coal reservoir rock porosity results in larger mineral content, elevated P wave velocity, and reduced S wave velocity, as shown in Figs. 8(c)-8(d). The sensitivities of P and S wave velocity to mineral content and porosity are different. Mineral content has a great influence on V_p , while porosity has a great influence on V_s . Fig. 8(e) shows the trend of V_p/V_s together with porosity: the V_p/V_s ratio increases with porosity, and this trend is more obvious than that under ideal conditions without minerals.

3.3.2 Effect of gas saturation

Simulation results under increasing gas saturation and actual conditions, while considering the influence of minerals,

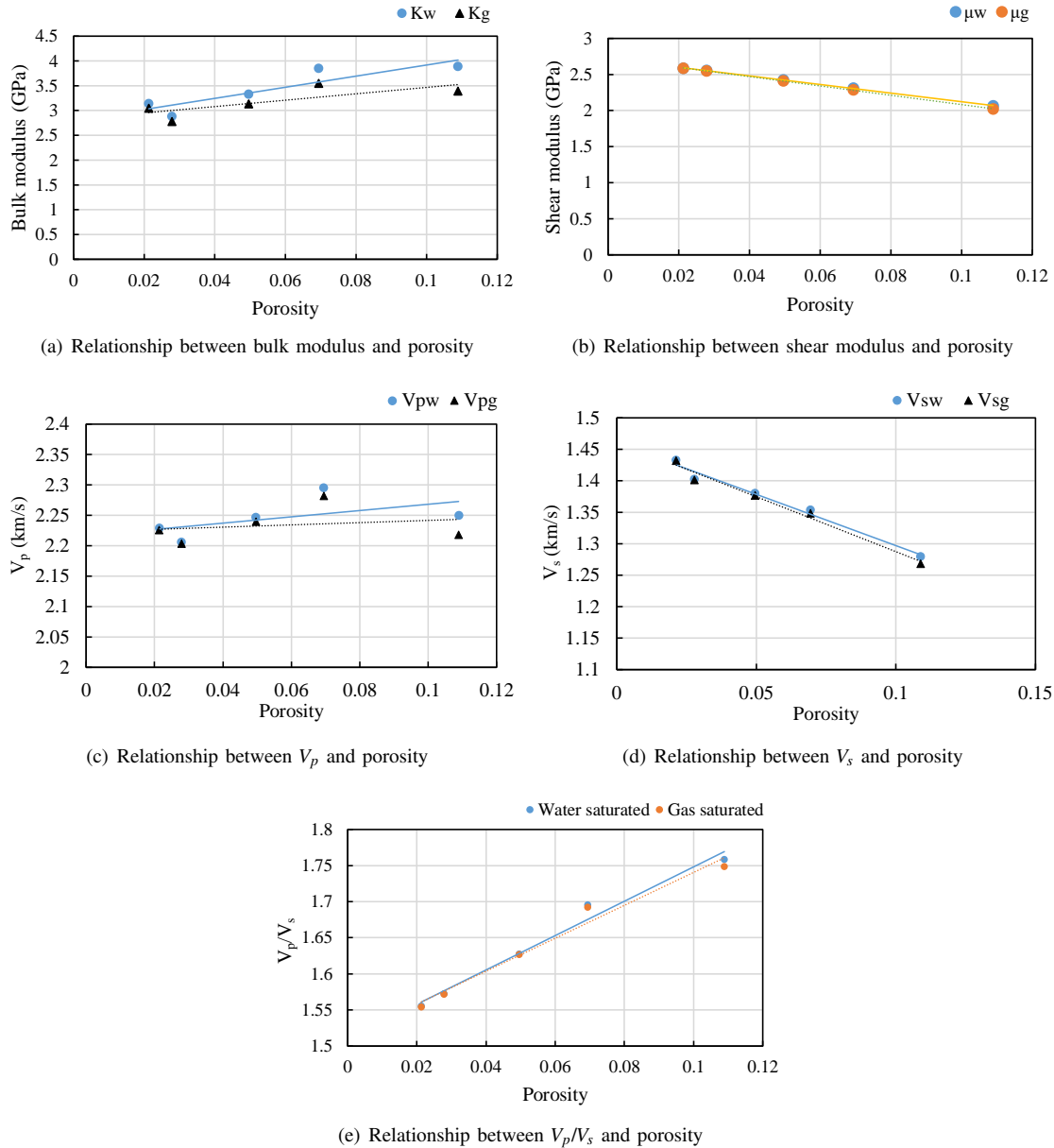


Fig. 8. Effect of porosity on elastic properties under real conditions.

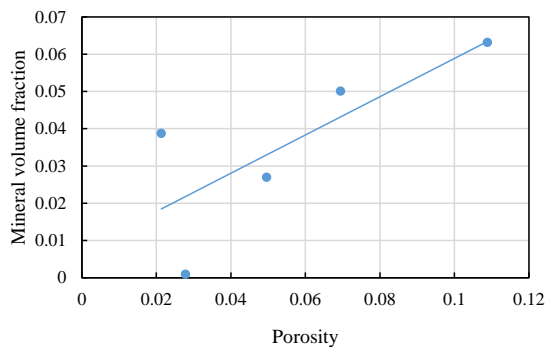


Fig. 9. Relationship between porosity and mineral volume fraction.

are shown as in Figs. 10(a)-10(b). The bulk modulus grad-

ually decreases, and the shear modulus remains basically unchanged. This is because gas and water have different bulk moduli and similar shear moduli with very small values near 0. It can be concluded that gas saturation has a greater effect on the bulk modulus than it does on the shear modulus.

The effect of gas saturation on V_p and V_s are shown in Figs. 10(c)-10(d). With increasing gas saturation, V_p declines while V_s stays constant, and the V_p/V_s ratio slightly subsides, as indicated in Fig. 10(e).

4. Conclusions

Digital rock physics are useful to help us better understand rock physical characteristics. In this paper, the elastic moduli of coalbed methane reservoir rock were simulated under different conditions based on three-dimensional digital core models

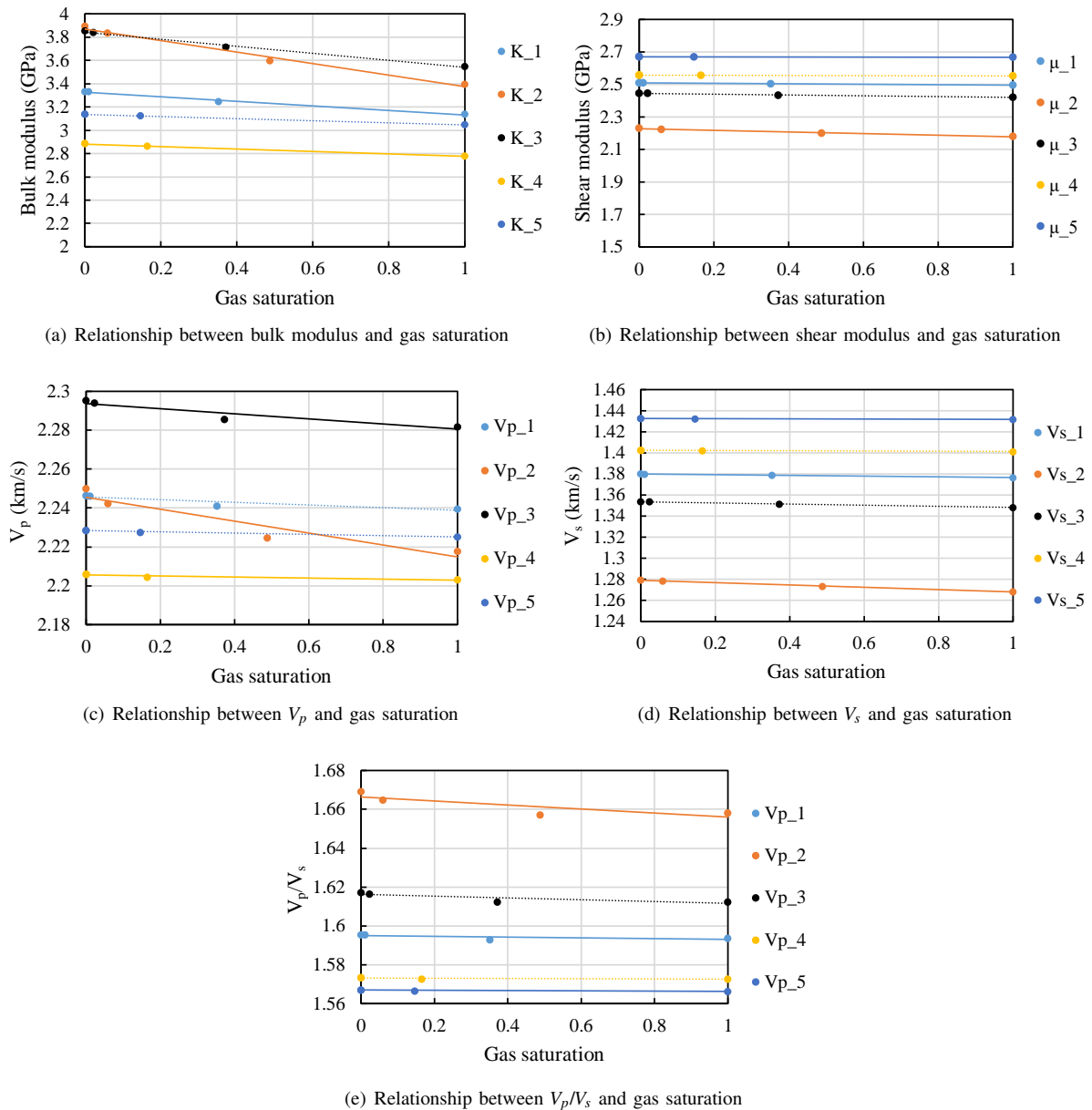


Fig. 10. Effect of gas saturation on elastic properties under real conditions.

and FEM modeling. The P wave velocity and S wave velocity of the core were also calculated. Based on our findings, the following conclusions are drawn:

- 1) Under the ideal condition of the lack of filling minerals, V_p and V_s of the cores gradually decline with rising porosity. Under actual conditions considering filled minerals, however, increasing porosity results in a gradually decline of V_s while V_p of the core gradually rises, which is an unexpected result. This is due to coalbed minerals developing mostly in the microfractures and some large pores, therefore porosity and mineral content are always positively correlated.
- 2) Under both ideal and real conditions, when gas saturation increases, V_p declines and V_s remains unchanged; the fluid almost has no contribution to the shear modulus.

- 3) Nevertheless, these results can improve our understanding of rock elastic behaviors in the coalbed. Our study was limited to conditions of one specific temperature and pressure, thus pressure and temperature still need to be considered in more detailed subsequent studies, since the gas elastic properties and adsorbed gas content are closely related to these two conditions. Moreover, anisotropy is also a crucial factor to consider in future research.

Acknowledgement

This study was financially supported by the National Natural Science Foundation of China (No. 41504094) and Open Foundation of Top Disciplines in Yangtze University (No. 2019KFJJ0818009). The authors would like to thank China Scholarship Council for the financial support for foreign stu-

dents, and they greatly appreciate the help of four anonymous reviewers for their constructive comments and suggestions.

Conflict of interest

The authors declare no competing interest.

Open Access This article is distributed under the terms and conditions of the Creative Commons Attribution (CC BY-NC-ND) license, which permits unrestricted use, distribution, and reproduction in any medium, provided the original work is properly cited.

References

- Al-Marzouqi, H. Digital rock physics: Using CT scans to compute rock properties. *IEEE Signal Processing Magazine*, 2018, 35(2): 121-131.
- Andrä, H., Combaret, N., Dvorkin, J., et al. Digital rock physics benchmarks-part II: Computing effective properties. *Computers & Geosciences*, 2013, 50: 33-43.
- Arns, C. H. *The Influence of Morphology on Physical Properties of Reservoir Rocks*. Sydney, The University of New South Wales, 2002.
- Chauhan, S., Rühaak, W., Khan, F., et al. Processing of rock core microtomography images: Using seven different machine learning algorithms. *Computers & Geosciences*, 2016, 86: 120-128.
- Chen, X., Zhou, Y. Applications of digital core analysis and hydraulic flow units in petrophysical characterization. *Advances in Geo-Energy Research*, 2017, 1(1): 18-30.
- Combaret, N., Dvorkin, J., Glatt, E., et al. Digital rock physics benchmarks-part II: Computing effective properties. *Computers & Geosciences*, 2013, 50: 33-43.
- Cui, T., Moore, C., Raiber, M. Probabilistic assessment of the impact of coal seam gas development on groundwater: Surat Basin, Australia. *Hydrogeology Journal*, 2018, 26: 2357-2377.
- Dvorkin, J. Rock physics: Recent history and advances, in *Geophysics and Ocean Waves Studies* [Working Title], 2020.
- Garboczi, E. J., Day, A. R. An algorithm for computing the effective linear elastic properties of heterogeneous materials: Results for composites with equal phase poisson ratios. *Journal of the Mechanics and Physics of Solids*, 1995, 43: 1349-1362.
- Gentzis, T., Bolen, D. The use of numerical simulation in predicting coalbed methane producibility from the Gates coals, Alberta Inner Foothills, Canada: Comparison with Mannville coal CBM production in the Alberta Syncline. *International Journal of Coal Geology*, 2008, 74: 215-236.
- Haralick, R. M., Sternberg, S. R., Zhuang, X. Image Analysis Using Mathematical Morphology. *IEEE Transactions on Pattern Analysis and Machine Intelligence*, 1987, PAMI-9: 532-550.
- Hu, S., Hoffman, E. A., Reinhardt, J. M. Automatic lung segmentation for accurate quantitation of volumetric X-ray CT images. *IEEE Transactions on Medical Imaging*, 2001, 20(6): 490-498.
- Huang, T., Yang, G., Tang, G. A fast two-dimensional median filtering algorithm. *IEEE Transactions on Acoustics, Speech, and Signal Processing*, 1979, 27(1): 13-18.
- Icke, I., Hanchi, J., Haralick, R. M., et al. TR-2005001: Automatic target detection in E3D images using mathematical morphology techniques. Computer science technical reports, CUNY Academic Works, 2005.
- Liu, X., Sun, J., Wang, H. Numerical simulation of rock electrical properties based on digital cores. *Applied Geophysics*, 2009, 6: 1-7.
- Madonna, C., Quintal, B., Frehner, M., et al. Synchrotron-based X-ray tomographic microscopy for rock physics investigations. *Geophysics*, 2013, 78: D53-D64.
- Makarynska, D., Gurevich, B., Ciz, R., et al. Finite element modeling of the effective elastic properties of partially saturated rocks. *Computers & Geosciences*, 2008, 34: 647-657.
- Maximenko, A., Kadet, V. V. Determination of relative permeabilities using the network models of porous media. *Journal of Petroleum Science and Engineering*, 2000, 28(3): 145-152.
- Moore, T. A. Coalbed methane: A review. *International Journal of Coal Geology*, 2012, 101: 36-81.
- Nie, X., Zhang, C., Wang, C., et al. Variable secondary porosity modeling of carbonate rocks based on μ -CT images. *Open Geosciences*, 2019, 11: 617-626.
- Nie, X., Zou, C., Li, Z., et al. Numerical simulation of the electrical properties of shale gas reservoir rock based on digital core. *Journal of Geophysics and Engineering*, 2016, 13: 481-490.
- Peng, C., Zou, C., Zhou, T., et al. Factors affecting coalbed methane (CBM) well productivity in the Shizhuangnan block of southern Qinshui basin, North China: Investigation by geophysical log, experiment and production data. *Fuel*, 2017, 191: 427-441.
- Serra, J. *Image Analysis and Mathematical Morphology*. Academic Press, New York, USA, 1982.
- Sun, H., Vega, S., Tao, G. Analysis of heterogeneity and permeability anisotropy in carbonate rock samples using digital rock physics. *Journal of Petroleum Science and Engineering*, 2017, 156: 419-429.
- Sun, J., Zhao, J., Liu, X., et al. Pore-scale analysis of electrical properties in thinly bedded rock using digital rock physics. *Journal of Geophysics and Engineering*, 2014, 11: 055008.
- Vishal, V., Mahanta, B., Pradhan, S. P., et al. Simulation of CO₂ enhanced coalbed methane recovery in Jharia coalfields, India. *Energy*, 2018, 159: 1185-1194.
- Wang, H., Fehler, M. The wavefield of acoustic logging in a cased-hole with a single casing-Part I: A monopole tool. *Geophysical Journal International*, 2018, 212: 612-626.
- Wang, H., Tao, G., Shang, X. F., et al. Stability of finite difference numerical simulations of acoustic logging-while-drilling with different perfectly matched layer schemes. *Applied Geophysics*, 2013a, 10: 384-396.
- Wang, H., Tao, G., Zhang, K. Wavefield simulation and analysis with the finite-element method for acoustic logging while drilling in horizontal and deviated wells. *Geophysics*, 2013b, 78: D525-D543.
- Wei, D., Tong, W. Research on edge detection based on mathematical morphology algorithm. Paper Presented

- at Proceedings of 2010 International Conference on Optoelectronics and Image Processing, Haikou, China, 11-12 November, 2010.
- Wei, Y., Nie, X., Jin, L. Investigation of sensitivity of shale elastic properties to rock components based on a digital core technology and finite element method. *Arabian Journal of Geosciences*, 2018, 11: 224.
- Zhang, J. Research on image processing based on mathematical morphology. *Agro Food Industry Hi-Tech*, 2017, 28: 2738-2742.
- Zhang, W., Fu, L., Zhang, Y., et al. Computation of elastic properties of 3D digital cores from the Longmaxi shale. *Applied Geophysics*, 2016, 13: 364-374.
- Zhao, J., Chen, H., Li, N. The study of elastic properties of fractured porous rock based on digital rock. *IOP Conference Series: Earth and Environmental Science*, 2020, 514: 022022.
- Zhao, J., Sun, J., Liu, X., et al. Numerical simulation of the electrical properties of fractured rock based on digital rock technology. *Journal of Geophysics and Engineering*, 2013, 10: 055009.